

NONLINEAR VIBRATION AND BIFURCATIONS OF A BENDING-TWISTING ROTOR SYSTEM

Yuanhao Chen

School for Engineering of Matter, Transport & Energy, Arizona
State University
Tempe, AZ, 85287, USA

Xiya Wang and Yeyin Xu¹

School of Aerospace Engineering, Xi'an Jiaotong University,
Xi'an, Shaan Xi, 710049, China

Bin Chen

College of Power and Energy Engineering
Harbin Engineering University
Harbin, HLJ, 150000, China

Tieyan Wang

BaiCheng Meteorological Observatory
Baichen, Jilin, 137000, China

ABSTRACT

In this paper, a nonlinear dynamic system of a bending-twisting rotor is studied. Analytical prediction of nonlinear vibration and Bifurcations in such a nonlinear dynamic system are presented from the implicit mapping method. Bifurcations on vibration evolution are obtained and the stability of the corresponding vibrations are discussed by eigenvalue analysis. Period-doubling bifurcations occur when the rotating frequency varies. The frequency-amplitude characteristics of periodic motions exhibit the motion complexity in frequency domain. Illustrations are given for comparison of the analytical and numerical results of nonlinear vibrations. The obtained results can be used to control the bending-twisting rotor with environmental noise.

INTRODUCTION

Bending and twisting are usual in industrial rotor system and unstable bending and twisting may cause serious damage to the practical rotor. Establishing a mathematical model for the bending and twisting shaft system is generally the primary concern in research. Analyzing the structural characteristics of the bending and twisting rotor and establishing a corresponding mathematical model based on its physical properties enable describing the dynamic behavior of the rotor shaft system in torsional vibration. Daniel et al.^[1] developed a 16-degree-of-freedom nonlinear dynamic model of torsional vibration for a two-stroke low-speed diesel engine using the lumped mass method. The research utilized instantaneous torque results from the shaft system and artificial neural networks (ANNs) to identify and address shaft vibrations and faults related to

torsional vibration, such as efficiency loss, power imbalance, or fuel injection system malfunctions. Lu et al.^[2] discussed the cylinder block vibration issue in medium-speed diesel engines by establishing a nonlinear rotor dynamic model considering the coupling effect between shaft torsional vibration and fuel injection angle. The research introduced instantaneous speed and cylinder pressure, derived formulas for calculating three excitation forces causing engine cylinder block vibration, and loaded the updated excitation forces into a finite element model for vibration simulation. By adjusting the value of the advanced injection angle for cylinder block vibration optimization, the optimal value of the advanced injection angle was determined to be 29 degrees, resulting in a reduction of 3.60%, 2.72%, and 3.16% in cylinder block vibration in the X, Y, and Z directions, respectively, compared to the original value. Uspensky et al.^[3] developed a 16-degree-of-freedom nonlinear rotor dynamic system model, including two nonlinear torques. The study classified the excitation sources of the torsional vibration into two types: dynamic torque acting on the crankshaft and dynamic torque acting on the rotor of the electric generator. Wu et al.^[4] obtained the torsional vibration responses of the crankshaft-gearbox coupling system in nonlinear industrial rotor system. The bending and twisting engine system comprises a torsional vibration damper, two cylinders, and a flywheel. In the gearbox, one gear is connected to the flywheel via a clutch, and another gear is connected to the power output shaft via an elastic coupling. Han et al.^[5] discussed the fatigue fracture at the spindle connections caused by torsional vibration through establishing a dynamic model of the propulsion rotor system of a bending-twisting shaft. The model considered structural parameters such as coupling stiffness, shaft stiffness, coupling

¹ Contact author: xuyeyin@xjtu.edu

damping, and structural damping of the shaft. By adjusting design parameters to reduce torsional vibration, the research systematically analyzed the reasons of torsional vibration in ship propulsion shafts. Zambon et al.^[6] established a mathematical model of the bending-twisting shaft system to simulate the transient responses of torsional vibration caused by ice loads. The focus of the research was to obtain torque excitation characteristics between ice and propellers by analyzing the interaction process between ice and propellers and proposing a method of superimposing individual ice loads. Xue et al.^[7] established a dynamic model of a two-dimensional lumped-parameter planetary gear system for analyzing torsional vibration signals. The system comprises planetary gears, carrier arms, internal and external gear rings, and output loads. Then, variations in gear mesh stiffness and bearing stiffness were calculated using the finite element method. The study found that different planetary bearing faults generated specific waveform and frequency spectrum characteristics in the carrier arm angular velocity signal. Senjanović et al.^[8] discussed the torsional vibration of a bending-twisting rotor system by deriving a multi-degree-of-freedom torsional rotor model of the complete propulsion system using the Rayleigh-Ritz method. The research focused on the ignition sequence of each cylinder in the diesel engine and its influence on the contribution of harmonic components to the torsional vibration of the engine shaft system.

DISCRETE MAPPING METHOD

Considering the impact of nonlinear excitation forces from bearings on the dynamic characteristics of the rotor system, a bearing-rotor system model is developed, as illustrated in Figure 1:

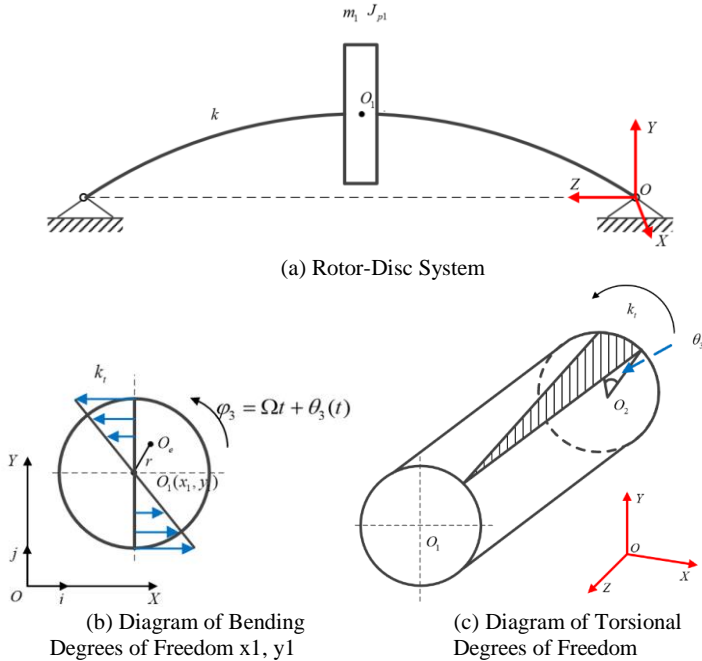


Fig.1 a physical model of a bending-twisting rotor

Establishing the physical model of the bending-twisting rotor considering nonlinear excitation forces from bearings, as shown in Equation (1).

$$\begin{aligned}
 & m_1 \ddot{x}_1 + c_1 \dot{x}_1 + k_1 x_1 + k_3 x_1 (x_1^2 + y_1^2) \\
 & - m_1 r [(\ddot{\theta}_3 - \theta_3 \Omega^2) \sin \Omega t + 2\dot{\theta}_3 \Omega \cos \Omega t] = m_1 r \Omega^2 \cos \Omega t \\
 & m_1 \ddot{y}_1 + c_2 \dot{y}_1 + k_2 y_1 + k_4 y_1 (x_1^2 + y_1^2) \\
 & + m_1 r [(\ddot{\theta}_3 - \theta_3 \Omega^2) \cos \Omega t - 2\dot{\theta}_3 \Omega \sin \Omega t] = m_1 r \Omega^2 \sin \Omega t \\
 & (J_{p1} + 2m_1 r^2) \ddot{\theta}_3 + c_3 \dot{\theta}_3 + k_3 \theta_3 - m_1 g \\
 & + (k_2 r y_1 \cos \Omega t - k_1 r x_1 \sin \Omega t) = T_\theta - m_1 g r \cos \Omega t
 \end{aligned} \tag{1}$$

In the above equation, m_1 and J_{p1} represent the mass and rotational inertia along the axis of rotation for the disc and shaft, respectively. k_1 and k_2 denote the bending stiffness of the rotor shaft, while k_3 and k_4 signify the support stiffness of the bearings. O_1 denotes the centroid of the disc, O_2 represents the center of mass of the disc, r stands for the eccentricity of the rotor system, x_1 and y_1 respectively denote the displacements of the rotor along the OX and OY axes, φ_3 represents the instantaneous angular displacement of the rotor about the OZ axis, and Ω signifies the angular velocity of the rotor.

Consider the nonlinear motions of the nonlinear rotor system in a small time interval where $t \in [t_{k-1}, t_k]$, Eq.(1) can be discretized with a midpoint scheme as^[9,10]:

$$\begin{aligned}
 x_{1,k} &= x_{1,k-1} + h x_{2,km} \\
 x_{2,k} &= x_{2,k-1} + h \left[E_{1,km} \cos \Omega t_{k+h/2} - \bar{k}_1 x_{1,km} \right. \\
 &\quad \left. - U_1 x_{2,km} - \bar{k}_2 x_{1,km} (x_{1,km}^2 + x_{3,km}^2) \right. \\
 &\quad \left. + (E_{2,km} - r \Omega^2 x_{5,km}) \sin \Omega t_{k+h/2} \right] \\
 x_{3,k} &= x_{3,k-1} + h x_{4,km} \\
 x_{4,k} &= x_{4,k-1} + h \left[E_{1,km} \sin \Omega t_{k+h/2} - g - \bar{k}_1 x_{3,km} \right. \\
 &\quad \left. - U_2 x_{4,km} - \bar{k}_2 x_{3,km} (x_{1,km}^2 + x_{3,km}^2) \right. \\
 &\quad \left. - (E_{2,km} - r \Omega^2 x_{5,km}) \cos \Omega t_{k+h/2} \right] \\
 x_{5,k} &= x_{5,k-1} + h x_{6,km} \\
 x_{6,k} &= x_{6,k-1} + h \left[\bar{T}_{km} - \begin{pmatrix} \bar{k}_2 r x_{3,km} \cos \Omega t_{k+h/2} \\ -\bar{k}_1 r x_{1,km} \sin \Omega t_{k+h/2} \end{pmatrix} \right]
 \end{aligned} \tag{2}$$

where

$$\begin{aligned}
 x_{i,km} &= \frac{x_{i,k} + x_{i,k-1}}{2}, \\
 t_k &= t_0 + kh, h = 2\pi / (f_1 N), k = 1, 2, \dots, N.
 \end{aligned} \tag{3}$$

The mapping structure in Eq.(2) defines the mapping as $P_k : \mathbf{x}_{k-1} \rightarrow \mathbf{x}_k$ ($\mathbf{x}_k = (x_{1,k}, x_{2,k}, x_{3,k}, x_{4,k})^T$, $k = 1, 2, \dots, N$). For

nonlinear solutions of the nonlinear rotor system, the global mappings have the form

$$\begin{aligned} P_1 : \mathbf{x}_0 &\rightarrow \mathbf{x}_1 \Rightarrow \mathbf{x}_1 = P_1 \mathbf{x}_0 \\ P_2 : \mathbf{x}_1 &\rightarrow \mathbf{x}_2 \Rightarrow \mathbf{x}_2 = P_2 \mathbf{x}_1 \\ &\vdots \\ P_N : \mathbf{x}_{N-1} &\rightarrow \mathbf{x}_N \Rightarrow \mathbf{x}_N = P_N \mathbf{x}_{N-1} \end{aligned} \quad (4)$$

consider a mapping structure of $P = P_N \circ P_{N-1} \circ \dots \circ P_2 \circ P_1$, where ‘◦’ represents the action between mappings. The corresponding algebraic equations of the mapping structure are in Eq.(2):

$$\mathbf{g}_k(\mathbf{x}_{k-1}, \mathbf{x}_{1,k-1}) = \mathbf{0} \quad (k=1,2,\dots,N) \quad (5)$$

where $\mathbf{g}_k = (g_{x_1,k}, g_{x_2,k}, g_{x_3,k}, g_{x_4,k})^T$ with

$$\begin{aligned} g_{1,k} &= x_{1,k} - x_{1,k-1} - h x_{2,km} \\ g_{2,k} &= x_{2,k} - x_{2,k-1} - h \left[\begin{array}{l} E_{1,km} \cos \Omega t_{k+h/2} - \bar{k}_1 x_{1,km} - U_1 x_{2,km} \\ -\bar{k}_2 x_{1,km} (x_{1,km}^2 + x_{3,km}^2) \\ + (E_{2,km} - r\Omega^2 x_{5,km}) \sin \Omega t_{k+h/2} \end{array} \right] \\ g_{3,k} &= x_{3,k} - x_{3,k-1} - h x_{4,km} \\ g_{4,k} &= x_{4,k} - x_{4,k-1} - h \left[\begin{array}{l} E_{1,km} \sin \Omega t_{k+h/2} - g - \bar{k}_1 x_{3,km} - U_2 x_{4,km} \\ -\bar{k}_2 x_{3,km} (x_{1,km}^2 + x_{3,km}^2) \\ - (E_{2,km} - r\Omega^2 x_{5,km}) \cos \Omega t_{k+h/2} \end{array} \right] \\ g_{5,k} &= x_{5,k} - x_{5,k-1} - h x_{6,km} \\ g_{6,k} &= x_{6,k} - x_{6,k-1} - h \left[\tilde{T}_{km} - \left(\begin{array}{l} \bar{k}_2 r x_{3,km} \cos \Omega t_{k+h/2} \\ -\bar{k}_1 r x_{1,km} \sin \Omega t_{k+h/2} \end{array} \right) \right] \end{aligned} \quad (6)$$

The periodicity condition of period- m waveforms is:

$$\begin{aligned} \mathbf{x}_N &= \mathbf{x}_0 \\ &\Rightarrow (x_{1,mN}, x_{2,mN}, x_{3,mN}, x_{4,mN}, x_{5,mN}, x_{6,mN})^T \\ &= (x_{1,0}, x_{2,0}, x_{3,0}, x_{4,0}, x_{5,0}, x_{6,0})^T \end{aligned} \quad (7)$$

The semi analytical solutions of period- m vibrations in the nonlinear rotor system can be achieved by solving the $6(mN+1)$ equations in Eq. (5) and (7). The initial conditions can be obtained from the symplectic integration method. Once the semi-analytical solutions of periodic vibrations are obtained, the stability and bifurcation analysis can be conducted by eigenvalue analysis.

Consider the perturbed equation of the discretized system as

$$\frac{\partial \mathbf{g}_k}{\partial \mathbf{x}_{k-1}}|_{(\mathbf{x}_{k-1}^*, \mathbf{x}_k^*)} \Delta \mathbf{x}_{k-1} + \frac{\partial \mathbf{g}_k}{\partial \mathbf{x}_k}|_{(\mathbf{x}_{k-1}^*, \mathbf{x}_k^*)} \Delta \mathbf{x}_k = \mathbf{0} \quad (8)$$

Transform Eq. (8) into

$$\Delta \mathbf{x}_k = DP_k \Delta \mathbf{x}_{k-1} \quad (9)$$

where

$$DP_k = \left[\frac{\partial \mathbf{x}_k}{\partial \mathbf{x}_{k-1}} \right]_{(\mathbf{x}_k^*, \mathbf{x}_{k-1}^*)^{(4 \times 4)}} \quad (10)$$

The disturbance $\Delta \mathbf{x}_N$ can be solved by

$$\Delta \mathbf{x}_{mN} = DP \Delta \mathbf{x}_0 = \underbrace{DP_{mN} \cdot DP_{mN-1} \cdots \cdot DP_2 \cdot DP_1}_{mN-\text{multiplication}} \Delta \mathbf{x}_0 \quad (11)$$

where

$$\begin{aligned} DP &= \left[\frac{\partial \mathbf{x}_{mN}}{\partial \mathbf{x}_0} \right]_{(\mathbf{x}_{mN}^*, \mathbf{x}_{mN-1}^*, \dots, \mathbf{x}_0^*)} = DP_{mN} \cdot DP_{mN-1} \cdots \cdot DP_2 \cdot DP_1 \\ &= \prod_{k=mN}^1 \left[\frac{\partial \mathbf{x}_k}{\partial \mathbf{x}_{k-1}} \right]_{(\mathbf{x}_{k-1}^*, \mathbf{x}_k^*)} \end{aligned} \quad (12)$$

The stability and bifurcations of period- m vibrations of the discrete nonlinear rotor system can be determined by the eigenvalues of DP

$$|DP - \lambda \mathbf{I}_{4 \times 4}| = 0 \quad (13)$$

The stability conditions are defined from the *discrete mapping method*.

- i. If all eigenvalues of DP are within the unit cycle (i.e. $|\lambda_i| < 1$, $i = \{1, 2, 3, 4, 5, 6\}$), the period- m waveforms is stable.
- ii. If at least one eigenvalue is out of the unit cycle (i.e. $|\lambda_i| > 1$, $i \in \{1, 2, 3, 4, 5, 6\}$), the period- m waveforms is unstable.
- iii. When there are eigenvalues on the unit cycle (i.e. $|\lambda_i| = 1$, $i \in \{1, 2, 3, 4, 5, 6\}$), bifurcation analysis is necessary for the nonlinear rotor system.

The bifurcations are defined as

- iv. If $\lambda_i = 1$ with $|\lambda_j| < 1$ ($i, j \in \{1, 2, 3, 4, 5, 6\}, i \neq j$), saddle-node bifurcation (SN) occurs.
- v. If $\lambda_i = -1$ with $|\lambda_j| < 1$ ($i, j \in \{1, 2, 3, 4, 5, 6\}, i \neq j$), period-doubling bifurcation (PD) occurs.
- vi. If $|\lambda_{i,j}| = 1$ ($i, j \in \{1, 2, 3, 4, 5, 6\}$), $\lambda_i = \bar{\lambda}_j$, Neimark bifurcation (NB) occurs.

NUMERICAL BIFURCATION DIAGRAM

In this part, the nonlinear bifurcation diagram of the period- m vibrations are performed. In the plots, the solid curve means the stable vibrations and the dashed curve means the unstable vibrations. The acronyms “SN”, “NB”, “PD” represent the saddle-node, Neimark and period doubling bifurcation, respectively. “P- m ” represents period- m nonlinear vibrations.

From Fig.2, it can be observed that the numerical solution of the bending-twisting rotor system exhibits synchronous periodic motions, period-2 motions, period-4 motions, and chaotic motions. Fig.2(a) illustrates the numerical bifurcation diagram of the velocity of the bending-twisting rotor in the x -direction. In the figure, besides the discrepancy between the amplitude of velocity and the displacement, the motions' trend are similar, exhibiting distinct intervals of period-2 motions, period-4 motions, and chaotic motions, and incomplete semi-analytical routes to connect each others. Additionally, discontinuities or broken lines are where unstable synchronous periodic motion happens and the excitation frequency difference are $\Omega \in (2.896, 2.898)$. The numerical solutions for period-2 motions and period-4 motions fail to form continuous curves to connect on bifurcation diagram.

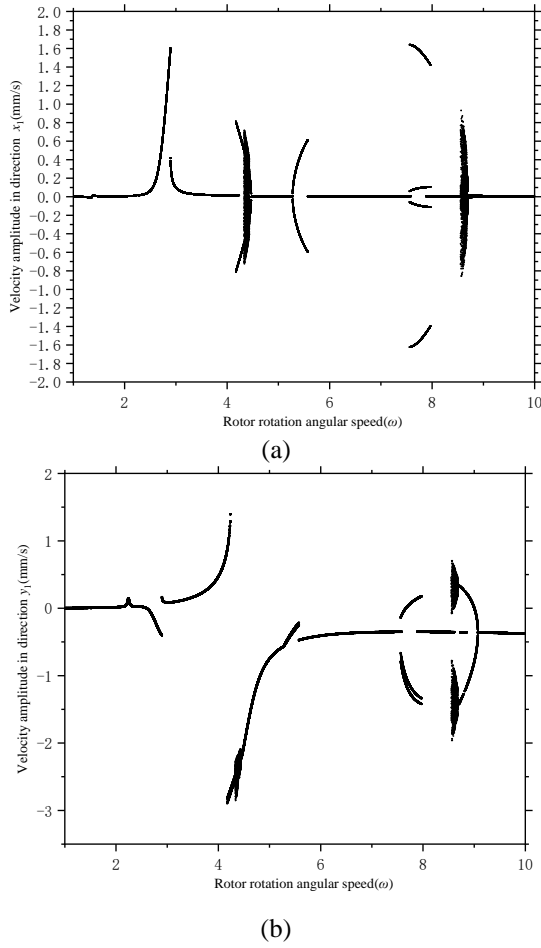


Fig.2 Numerical bifurcation diagrams of the coupled bending-torsional vibrations in the rotor system with varying the excitation frequency ($\Omega \in (0.0,10.0)$). (a) velocity in x -direction, (b) velocity in y -direction, (c) velocity of torsion.

Fig.2(b) illustrates the numerical bifurcation diagram of the velocity of the bending-twisting rotor in the y -direction. The pattern of the numerical bifurcation diagram is similar to the ones of y_1 , except for the development routes from period-4

motions motions to other higher order periodic motions, which requires further confirmation through data analysis. It can be observed that the bending-twisting rotor system exhibits two chaotic motions within $\Omega \in (1,10)$. However, influenced by gravitational factors and support stiffness, the bending-twisting rotor system's period-2 motions tends to disappear near chaotic motion, while the period-4 motions tend to evolve towards period-8 motions motion. Fig.2(c) illustrates the numerical bifurcation diagram of the twisting angles of the bending-twisting rotor in the twisting direction.

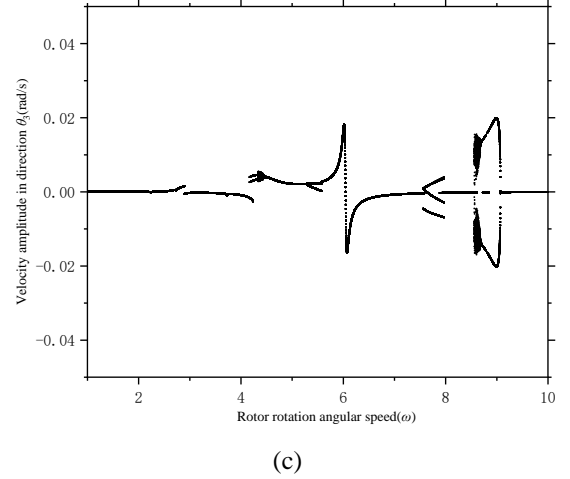
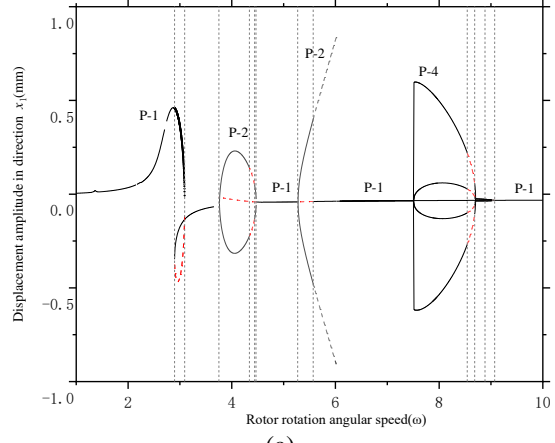


Fig.2 continued.

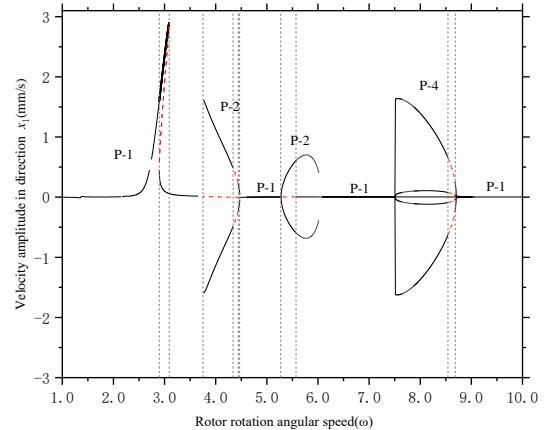
In Fig.3, the solid black lines represent stable periodic motion while the dashed red lines represent unstable periodic motion. Fig.3(a) depicts the predicted semi-analytical motions for the displacement x_1 of the bending-twisting rotor system. In the figure, synchronous periodic motion comprises two independent unstable speed regions, $\Omega \in (2.896, 3.091)$ and $\Omega \in (5.271, 5.571)$, and two mixed unstable regions, $\Omega \in (3.751, 4.467)$ and $\Omega \in (8.885, 9.071)$. period-2 motions encompass one unstable speed region, $\Omega \in (4.341, 4.44)$. Period-4 motions include one unstable region, $\Omega \in (8.542, 8.685)$. Fig.3(b) illustrates the semi-analytical solution for the velocity of x_1 of the bending-twisting rotor. In the figure, the unstable regions contained within synchronous periodic motions, period-2 motions and period-4 motions are consistent with those in the displacement direction. Fig.2(c) presents the semi-analytical solution for the displacement of y_1 of the bending-twisting rotor. As depicted, the independent unstable speed regions for synchronous periodic motion are $\Omega \in (2.896, 3.091)$ and $\Omega \in (4.341, 4.44)$. Additionally, a comparison with the semi-analytical solution of x_1 reveals the disappearance of the period-2 motions within speed region $\Omega \in (4.341, 4.44)$, indicating the potential transition from

unstable synchronous periodic motion to unstable period-2 motion in this region, which requires further assessment based on the characteristics of bifurcation points. Moreover, within speed regions $\Omega \in (7.228, 8.704)$ and $\Omega \in (8.542, 8.704)$, there are instances of unstable period-2 motions transitioning to stable period-4 motions and unstable period-2 motions, respectively. The specific circumstances also necessitate further judgment based on the characteristics of bifurcation points. Fig.3(d) presents the semi-analytical solution for the velocity of y_1 of the bending-twisting rotor system. Compared to the results for displacement y_1 , the velocity results exhibit similar characteristics across the speed ranges $\Omega \in (3.751, 4.467)$ and x_1 as the semi-analytical solutions for displacement.

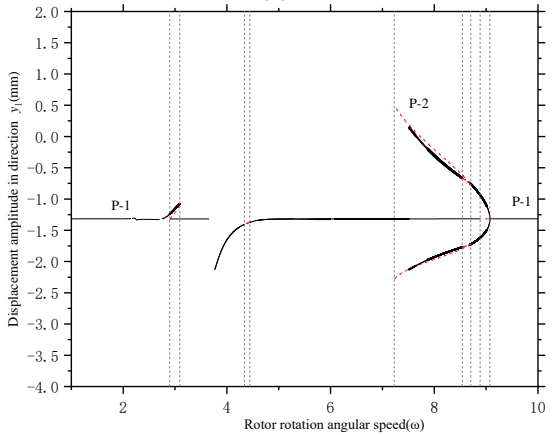
Additionally, within the speed range $\Omega \in (7.228, 9.071)$, there exists a complete semi-analytical path from stable synchronous periodic motion to unstable period-2 motion, then to period-4 motion, and finally back to stable synchronous periodic motion. Fig.3(e) and 3(f) depict the semi-analytical solutions for the displacement and velocity, respectively, in twisting direction of the bending-twisting rotor system. From the figures, it can be observed that the bending-twisting rotor system exhibits a more complex semi-analytical path in the torsional vibration direction. Besides the unstable speed regions for bending vibration mentioned above, in the speed range $\Omega \in (5.571, 6.015)$, there exist mixed unstable synchronous periodic motion and stable period-2 motion for torsional vibration.



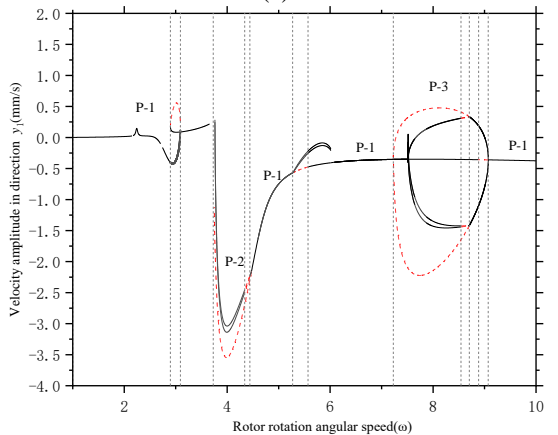
(a)



(b)



(c)



(d)

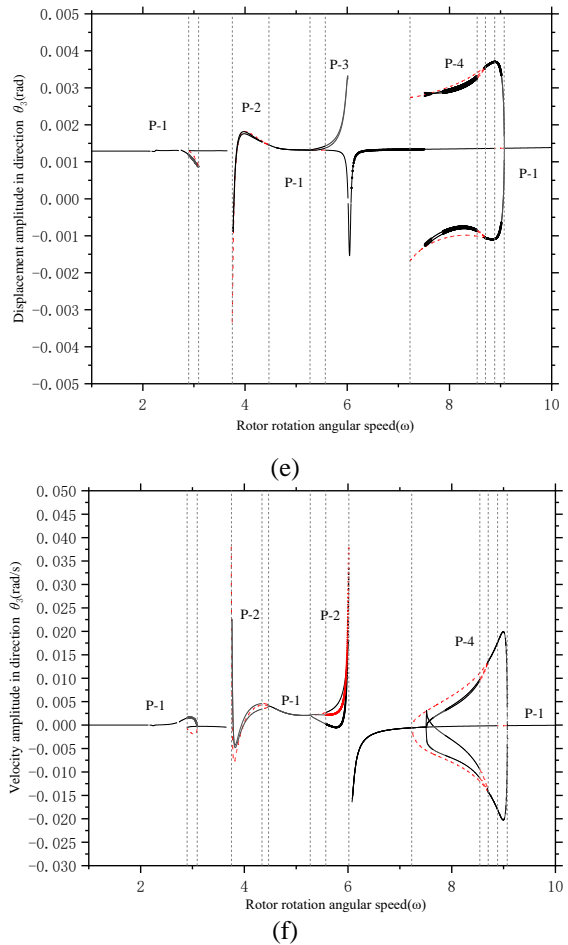


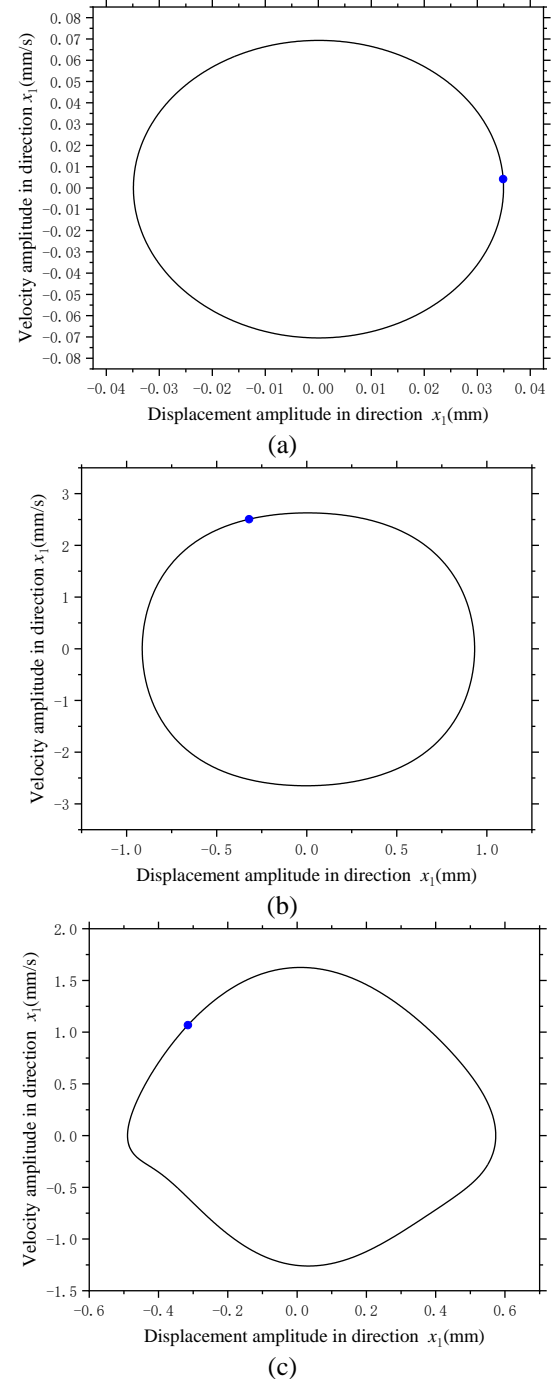
Fig.3 Semi-analytical bifurcation diagrams of the coupled bending-torsional vibrations in the rotor system with varying the excitation frequency ($\Omega \in (0,10.0)$). (a) velocity in x -direction, (b) velocity in y -direction, (c) velocity of torsion.

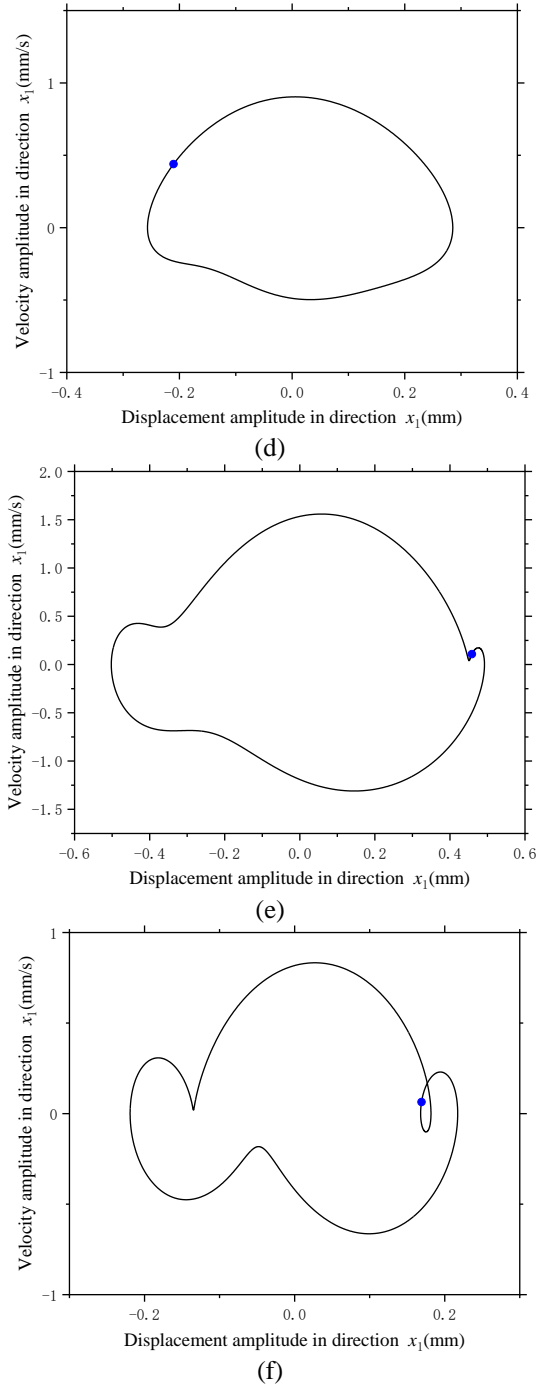
NONLINEAR VIBRATION ILLUSTRATION

Figure 4 illustrates the phase trajectories of the semi-analytical predictions for the bending-twisting rotor system in the x_1 direction. Specifically, Fig.4(a), (c), and (e) depict phase trajectories of stable periodic solutions of period-1, period-2, and period-4, respectively, while Fig.4 (b), (d), and (f) illustrate phase trajectories of unstable periodic solutions period-1, period-2, and period-4, respectively.

From the comparison of Fig.4(a), (c), and (e), it can be observed that the trajectory of periodic motion of the bending-twisting rotor system in the x_1 direction transitions from standard synchronous periodic motion to non-standard elliptical periodic motion from period-1 to period-4. This phenomenon indicates that the path of development from synchronous periodic motion to higher-order periodic motion in the x_1 direction for the bending-twisting rotor system is not evident. Furthermore, from the comparison of unstable solutions in Fig.4.(b), (d), and (f), it is noted that the path of transition from synchronous periodic motion to higher-order periodic motion in

the x_1 direction for the bending-twisting rotorsystem is similarly not distinct. However, the system exhibits more pronounced irregular motion and trajectory distortion in unstable solutions, leading to instability issues in system operation.





trajectories of unstable periodic solutions period-1, period-2, and period-4, respectively.

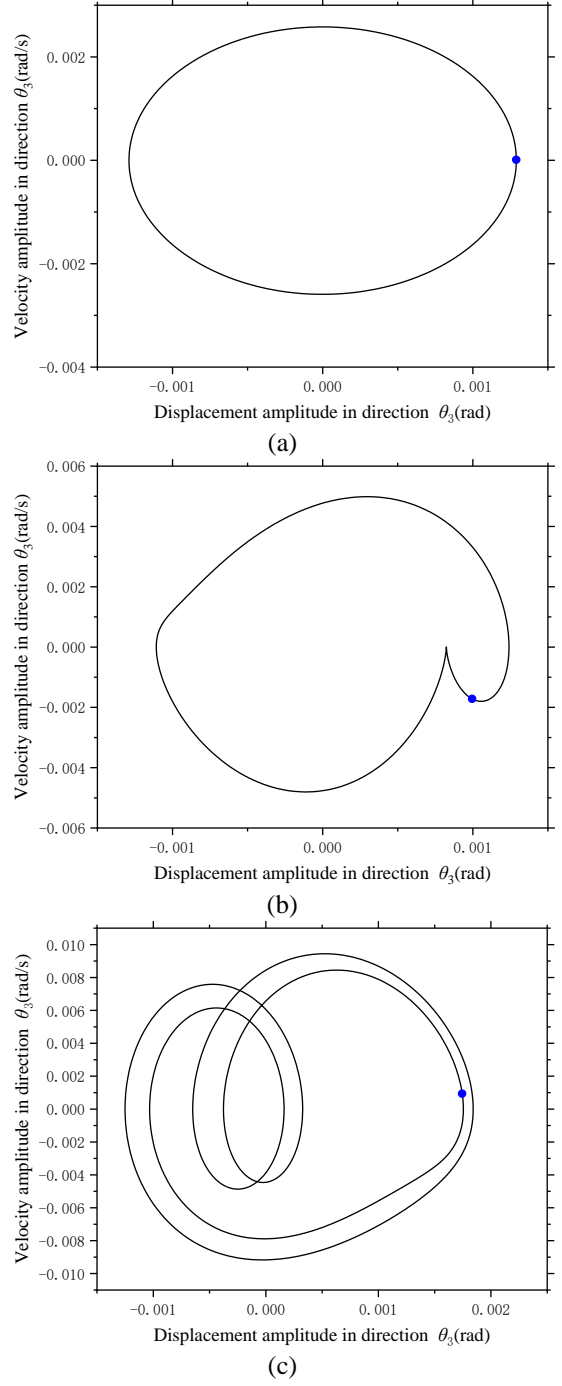


Fig.4 Nonlinear motion illumination of period-1 vibration in the rotor system. (a) stable period-1, (b) unstable period-1, (c) period-2, (d) unstable period-2, (e) stable period-4, (f) unstable period-3.

Figure 5 depicts the phase trajectories of the semi-analytical predictions for the bending-torsion coupled periodic motion of the bending-twisting rotor system in the twisting direction. Specifically, Fig.5 (a), (c), and (e) illustrate phase trajectories of stable periodic solutions period-1, period-2, and period-4, respectively, while Fig.5 (b), (d), and (f) depict phase

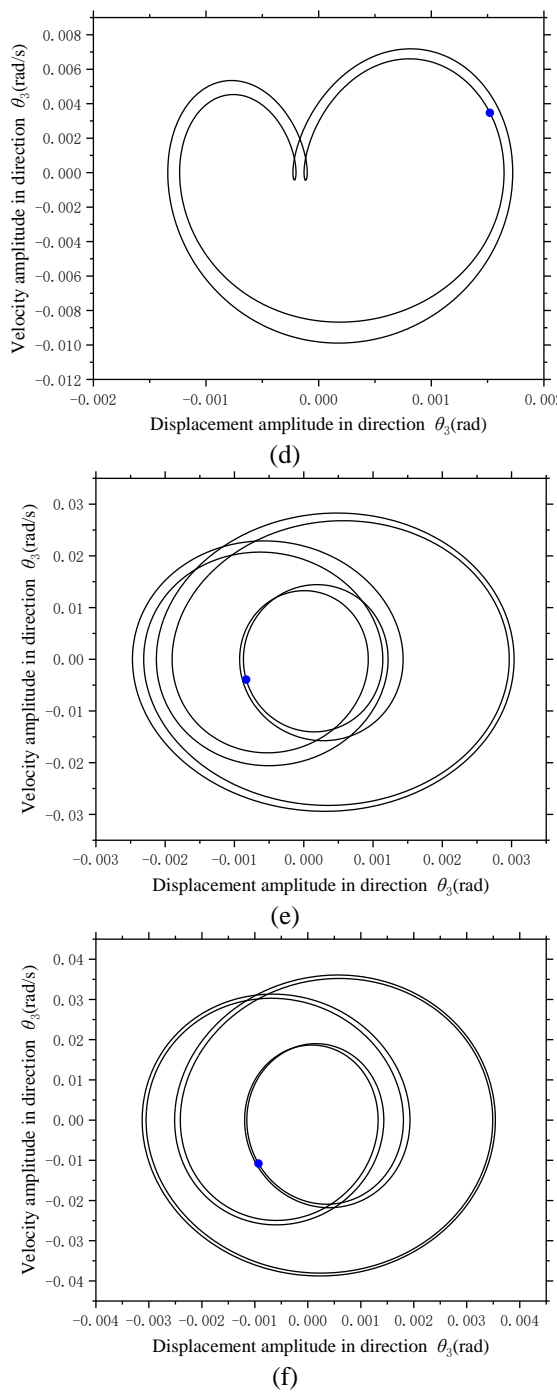


Fig.5 Nonlinear motion illumination of period-1 vibration in the rotor system. (a) stable period-1, (b) unstable period-1, (c) period-2, (d) unstable period-2, (e) stable period-4, (f) unstable period-3.

From Fig.5(a), (c), and (e), it is evident that in the twisting direction, the bending-twisting rotor system exhibits complete periodic motion trajectories from period-1 to period-2 and then to period-4. This result indicates that the vibration signal of the bending-twisting rotor system in the twisting direction is most suitable as a reference indicator for the nonlinear periodic motion of the system leading to chaos. Meanwhile, similar to

unstable periodic solutions in the x_1 and y_1 directions, significant vibration distortion phenomena also exist in the twisting direction for unstable solutions.

CONCLUSIONS

This research establishes the dynamic equations governing the bending-torsion coupled motion of the nonlinear rotor system. Subsequently, employing the discrete mapping method, semi-analytical motions for the nonlinear bending-twisting rotor system is constructed as a sequence of discrete vector points. The stability of the discrete periodic motions is determined based on the eigenvalues of the global Jacobian matrix of the rotor system. Additionally, numerical solutions of the bending-twisting rotor system in each degree of freedom direction are obtained using traditional numerical methods to construct numerical Poincaré mappings, which are then compared and analyzed against the results obtained from the semi-analytical approach developed in this research. The results demonstrate that the semi-analytical motions not only effectively agree with the results obtained from numerical simulations but also provide unique motions in the unstable speed region.

ACKNOWLEDGEMENT

This work is supported by the National Nature Science Foundation of China (Grant No. 12102319) and the Key R&D and Transformation Plan Project of Qinghai Province(NO. 2023-QY-215).

REFERENCES

- [1] Daniel Palomo Guerrero, Francisco J. Jiménez-Espadafor. Torsional system dynamics of low speed diesel engines based on instantaneous torque: Application to engine diagnosis. *Mechanical Systems and Signal Processing*,2019(116): 858-878.
- [2] Shiyi Lu, Yuxuan Chen, Haifeng Cao, et al. Coupling effect of shaft torsional vibration and advanced injection angle on medium-speed diesel engine block vibration. *Engineering Failure Analysis*,2023(154): 107624.
- [3] B. Uspensky, K. Avramov, B. Liubarskyi, et al. Nonlinear torsional vibrations of electromechanical coupling of diesel engine gear system and electric generator. *Journal of Sound and Vibration*,2019(460): 114877.
- [4] Kun Wu,Zhiwei Liu,Qian Ding, et al. Torsional vibration responses of the engine crankshaft-gearbox coupled system with misfire and breathing slant crack based on instantaneous angular speed. *Mechanical Systems and Signal Processing*,2022(173): 109052..
- [5] Hyung Suk Han, Kyoung Hyun Lee, Sung Ho Park. Parametric study to identify the cause of high torsional vibration of the propulsion shaft in the ship. *Engineering Failure Analysis*,2016(59): 334-346..
- [6] Alessandro Zambon, Lorenzo Moro. Torsional vibration analysis of diesel driven propulsion systems: The case of a polar-class vessel. *Ocean Engineering*,2022(245): 110330.
- [7] Song Xue, Ian Howard, Congsi Wang, et al. The diagnostic analysis of the planet bearing faults using the torsional vibration signal. *Mechanical Systems and Signal Processing*,2019(134): 106304.

- [8] Ivo Senjanović, Neven Hadžić, Lech Murawski, et al. Analytical procedures for torsional vibration analysis of ship power transmission system[J]. *Engineering Structures*, 2019(178): 227-244.
- [9] Luo, Albert Chao Jun, 2015, “Discretization and implicit mapping dynamics”, *Springer Berlin Heidelberg*.
- [10] Luo, Albert Chao Jun, 2015, “Periodic flows to chaos based on discrete implicit mappings of continuous nonlinear systems”, *International Journal of Bifurcation and Chaos*, **25**(3), pp:1550044.